Structural integrity analysis of the pre-stressed concrete dome of the Belgrade fair hall 1

Mirjana Jelić
Intellectual Property Office of the Republic of Serbia, Kneginje Ljubice 5, 11000 Belgrade, Serbia
Mjelic@zis.gov.rs

Aleksandar Sedmak
Faculty of Mechanical Engineering in Belgrade, University of Belgrade, Kraljice Marije 16, 11000 Belgrade, Serbia
Faculty of Civil Engineering, University of Brasov, Turnului 5, 500152 Brasov, Romania
asedmak@mas.bg.ac.rs, https://orcid.org/0000-0002-5438-1895

Boris Folić, Simon Sedmak
Innovation Centre of Faculty of Mechanical Engineering, Kraljice Marije 16, 11000 Belgrade, Serbia
boris.r.folic@gmail.com, https://orcid.org/0000-0003-2127-0264
simon.sedmak@yahoo.com, https://orcid.org/0000-0002-2674-541X

Mihajlo Arandjelović
Innovation Centre of Faculty of Mechanical Engineering, Kraljice Marije 16, 11000 Belgrade, Serbia
Faculty of Civil Engineering, University of Brasov, Turnului 5, 500152 Brasov, Romania
msarandjelovic@mas.bg.ac.rs, https://orcid.org/0000-0002-5040-5167

Radomir Folić
Faculty of Technical Sciences, University of Novi Sad, Serbia
folic@uns.ac.rs

Dorin Radu
Faculty of Civil Engineering, University of Brasov, Turnului 5, 500152 Brasov, Romania
dorin.radu@unitbv.ro, https://orcid.org/0000-0001-5043-27

Citation: Jelić, M., Sedmak, A., Folić, B., Sedmak, S., Aranđelović, M., Folić, R., Radu, D. Structural integrity analysis of the pre-stressed concrete dome of the Belgrade fair hall 1, Frattura ed Integrità Strutturale, 67 (2024) 337-351.

Received: 01.09.2023
Accepted: 10.12.2023
Online first: 16.12.2023
Published: 01.01.2024

KEYWORDS. Belgrade fair hall 1, Structural integrity, Pre-stressed concrete, Numerical simulation.

INTRODUCTION

Through the history of a mankind, large structures were always a demonstration of power and human ingenuity to make them bigger and bigger, but also more reliable at the same time, [1]. Concrete was always a suitable material for large structures, due to its low price and satisfying mechanical properties, except for the tensile strength. This is why innovative solutions, such as pre-stressed or reinforced concrete, were necessary to make larger spans for bridges and larger diameters for self-supporting domes possible.

(Several studies are concerning the design and structural behaviour of concrete domes, but few are dealing with structural integrity topic. Thus, in 1983 Zarghamee et al are proposing a design procedure for determining the buckling strength of concrete domes with prestressed concrete edge rings is presented. This procedure was developed using a conceptual model for predicting the buckling strength of concrete domes based on the available literature on stability of spherical shells and creep of concrete [2]. The model is based on the assumption that the dome contains geometric imperfections in the form of spherical caps with different curvature radius.

In same year (1983), Ashar and Naus [3] are presenting an overview of the use of prestressed concrete domes in U.S. nuclear plants, highlighting the major problems which have been encountered with prestressed concrete con-struction at nuclear power plant containments: dome delamination, cracking of anchorheads, settlement of bearing plates. The study concludes with the need of structural integrity assessment for the existing concrete dome like structures. Additional examples of construction, rehalibitation and maintenance of prestressed concrete structures can be found in [4].

In 2017 Moncarz et al. [5] are investigating the collapse causes of a reinforced concrete dome, by means of structural integrity approach, analysing the influence of concrete cracks due temperature and shrinkage stresses.

In this paper we focus attention to the largest pre-stressed self-supporting dome in the world, sitting proudly on the top of Belgrade fair hall No. 1 ever since its construction in 1957. It was the world's largest dome between 1957 and 1965 and is still Europe's largest dome, as well as the largest dome in the world made of pre-stressed concrete, [6].

Belgrade fair hall 1, is the exhibition hall of the Belgrade Fair, and with height 27.8 m and diameter 106 m, Fig. 1a. The outer outline of the hall is made of upper peripheral galleries, at heights of 4.7 and 8.7 m. The hall is surrounded by glass walls with a diameter 117 m. It comprises the dome and supports, bearing the roof dead load, with a 97.5 m diameter; the gallery and its supports; and the basement and ground floor [7]. Central circular cap is slightly convex and double plated with thickness 8 cm each and whose surfaces are connected by circular and radial ribs.

It was designed by a team comprising an architect Milorad Pantović and civil engineers Branko Žeželj, Boško Petrović and Dimitrije Ćertić, and tested using the model 1:10, Fig. 1b, [7]. After testing of the Hall 1 1:10 model, the following was concluded, [7]:

- Under symmetrical load, compressive stresses would be critical;

- Under asymmetrical load, also bending and tensile stresses would occur;
- Anyhow, not even 2.5 larger load than the design load due to snow would result in considerable tensile stresses.

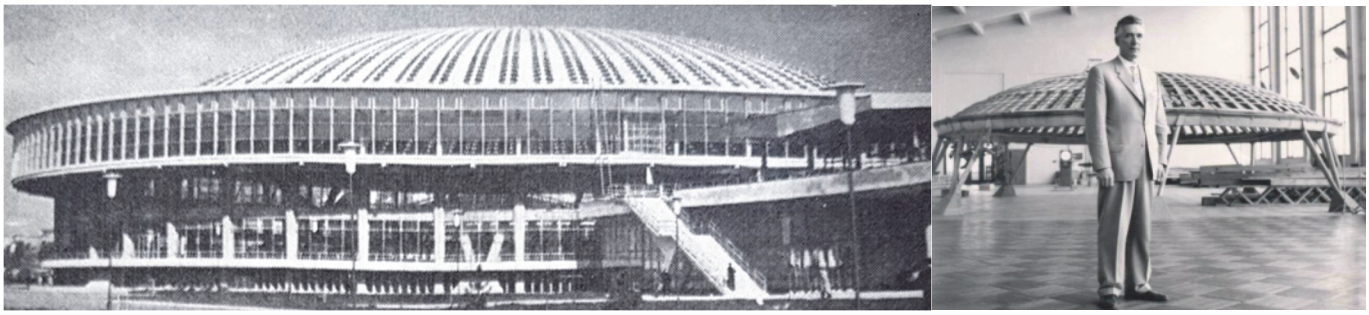

Figure 1: a) Belgrade fair hall 1, b) model 1:10 with Branko Žeželj in front of it [6].

Such a favourable stress state was obtained thanks to the pre-stressing, significantly reducing tension stresses. The hoop structure was subjected to positive bending moments in the vertical planes (around the second axis), in the sections between the "V" columns (portions of the full span), along with negative moments in the cross-sections above these supports (sections above the "V" columns), [6-8]. Maximum moment in vertical planes (around the second axis) reached 1314 tm, while its negative counterpart was 1105 tm. Maximum bending moments in the horizontal plane (around the third axis) were 533 tm, and highest negative moments were -536 tm. In addition, significant torsion moments (156 tm) were present, along with shear stresses, [6,7].

In paper [9] the pre-stressing cable distribution along the cross-section of the hollow concrete support ring was shown (Fig. 4, [10]). A total of 142 cable groups (each cable comprises 6 wires of 5 mm in diameter) were placed around the ring structure in order to cover the horizontal loads. For the purpose of bearing vertical negative bending moments above the top ring plate above the "V" columns, a total of 64 cable groups were installed, whereas 60 cable groups were used in the bottom plate, along its full span, whose purpose was to carry the vertical positive bending moments. Another cable group was placed in the ring rib to carry on the tensile stresses around the "V" columns, [7,9].

In this paper, calculations made during design of Hall 1, are repeated using recently developed methods, which were not available then. Therefore, we start with the comparison of results obtained following finite element analysis (FEA) with SAP2000 and TOWER software, with results which obtained by analytical calculation of a 1:10 scale model, as done originally by Branko Žeželj, [7].

The dome system consists of the following structural sub-assemblies/elements:

- Central circular reinforced concrete cap, with a diameter of 27 m.
- 80 precast elements reinforced concrete semi-arched ribs of I-profile with a length of 35 m, each weighing 34 tons.

The following elements were used as support for the central circular cap:

- Pre-stressed hollow concrete support ring with a trapezoid cross-section, with a diameter of 94 m. This ring supports the prefabricated semi-arched ribs made of reinforced concrete
- Three middle rings placed between the central circular cap and ring.
- The ring is supported by 8 V-shaped columns.

Finally, in this paper a new approach to analysis of large constructions is presented, based on the structural integrity assessment of the cracked pre-stressed concrete dome, using numerical simulation by the Finite Element Method (FEM). Toward this aim, an artificially introduced crack was analyzed in respect to potential effects of its growth. Large number of different calculations were performed to take into account different loading and supporting conditions, including numerical simulation of crack growth in a support column.

MATERIALS AND METHODS

Concrete used for the dome had compressive strength of 450 kg/cm², after 28 days (which is a period required for fresh concrete to harden enough to reach it's intended load-bearing capacity, under normal atmospheric conditions). Steel wire for pre-stressing had tensile strength of 1500 MPa and its yield stress was 1250 MPa, as given in originally used units, [6,7]. Aforementioned value of concrete strength corresponds to 45 MPa, whereas yield stress value and tensile strength values for the steel wire correspond to 1250 MPa and 1500 MPa, respectively. These values were used as input data for the

FEM calculations. Regarding concrete, one should keep in mind potential degradation of its properties, as described in [10]. Anyhow, since none of the mechanisms described in [11] are present in our case, the properties were taken as defined in [5,6]. Based on provided data, dome deflections were analyzed under symmetrical and asymmetrical loads, and were compared to deflections measured on the test model (1:10 scale). After this stage was completed, two numerical simulations were performed, using the finite element method, the first one taking into account the dome as a whole, using SAP2000 and TOWER software, and the second one, taking into account an assumed crack, and thus using specialized FE software ABAQUS v6.17, as described in [8, 11-22] for different structural integrity problems, including pressure vessels and risk analysis, [11-13], welded joints, [14-16], hip implants, [17], and civil engineering structures, [18-21]. The first model was then used to compare the results with original ones, as given in [7], whereas the second one was used to assess structural integrity of the dome. In any case, it was the stress and strain state that is calculated by using the finite element method (FEM) and its extended version, XFEM, to simulate crack growth, as applied in [22-25] and explained in [26].

NUMERICAL SIMULATIONS OF THE DOME AS A WHOLE

To model Hall 1 the TOWER software was used, whereas SAP2000 was used to calculate the reaction forces in the dome as shown in [9]. SAP 2000 software was used for this purpose since it works better with more complex geometries and problems in general, while being intuitive and easy to use. Semi-arch shapes were varied, along with the changes in the cross-sections along the arch lengths. Adopted arches were slightly stronger than the ones shown in [1,6], with a parabolic arch. It was determined that the reaction forces in the semi-arches from the dome dead weight acting on the main support ring was 1050 kN, i.e. that the vertical load was p_v = 140 kN/m', whereas the horizontal load was p_h = 247.8 kN/m'.

Due to potential problems related to TOWER software during simulation of complicated pre-stressing loads, especially if geometry is not symmetrical one, a cross-section of the support ring was adopted in a way as close to the real one as possible, which can be seen in Fig. 2. In addition, a local coordinate system (LCS) had to be adopted, wherein vertical plate bending of the support ring corresponded to bending about the second axis. Considering that the adopted cross-section of the support ring was not symmetric, one part of the support ring had one coordinate system, whereas the other part had its own coordinate system, which is rotated by 90 or 180° (or by any other angle) relative to the first one, as shown in Fig. 3.

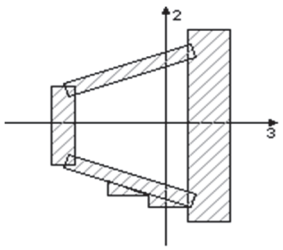

Figure 2: Support ring cross section in the local coordinate system.

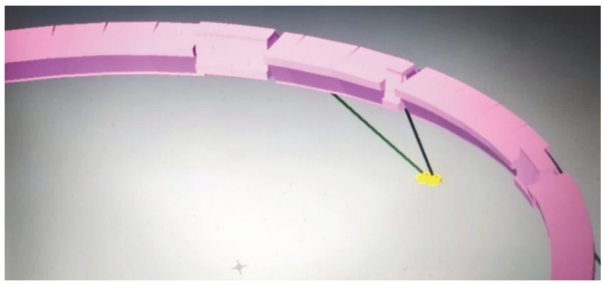

Figure 3: Different orientations of local coordinate systems in a 3D representation of support ring.

More details about the FE modelling of the dome as a whole are given in [8]. These calculations considered various approximations, due to structure symmetry - it was assumed vertical displacements did not exist within the dome, that semi-arched ribs were fixed at their bottom ends in the concrete support ring, and that they were hinged at the top ends in the central circular cap. In addition, the load on the dome was taken as evenly distributed along its surface, as presented in [7,9]. The support ring was discretized using finite elements of average size 0.5 m, to make diagram interpretation easy, e.g. in the case of forces in the areas above the columns and the full span. However, changes in the local coordinate system orientation during certain pre-stressing stages may provide erroneous results. Therefore, special configuration was adapted to the pre-stressing stages, leaving only one location where transversal forces indicated non-realistic difference for a single group of bottom section cables.

In this model, cables were introduced in the initial anchoring moment, so no additional force loss was not taken in account. In order to monitor the effects on the structure, various load cases shown in Tab. 1 were considered, consisting of different loads acting on the dome and the internal forces.

Case	Load
1	g - Dead load of the large support hoop and "V"columns
2	V- pv=140.00 kN/m - Dome load in vertical direction, distributed on the external hoop
3	H - ph=247.83 kN/m – The same as 2 but in horizontal direction
15	Pre-stressing initiation of middle group cables on the ring - Nko
16	The same as 15 for both zones and lengths on the ring bottom plate - Nko
17	The same as 15 for the ring top plate - Nko
22	The same as 16 and 17 plus the edge cables of the ring minus the inclined rib cables - Nko
23	1.00·g+1.13·(V+H) – The support ring/hoop dead load and "V"columns, as well as load from dome self weight load and snow load
24	All cables, except the inclined ones in the rib (of the support ring), are combined with the dead weight of top dome structure, snow, large support ring and "V" columns. Final moment of all pre-stressing force loss is combined with load case 23

Table 1: Load cases used in numerical analyses of the structure.

RESULTS

Tab. 2 shows extreme values obtained by simulations of loads at various critical locations within the model for load cases 1-3, whereas Tab. 3 show the same for load cases 15-17 and 22-24. These results include normal and transverse forces, bending moments and deformations (deflections).

Area	Above the "V"columns			Full span		
Load case	1	2	3	1	2	3
N [kN]	-1479.6	-1917.8	11722.15	-2252.7	-2934.56	11722.15
M_x [kNm]	-474.99	-718.62	-0.74	539.38	718.62	0.75
M_y [kNm]	5658.62	6676.14	-107.24	-4304.3	-6373.53	-107.24
M_z [kNm]	-2242.6	-2921.6	-5.59	2189.04	2851.7	2.65
T_2 [kN]	148.21	-814.88	-65.34	-625.53	193.08	65.34
T_3 [kN]	-535.58	-1899.13	0	1450.1	701.31	0
z [mm]	-35.8		1.47	-35.8		1.47
r_1 [mrad]	-0.39			0.79		

Table 2: Load cases 1, 2, 3 – Extreme values.

Area	Above the "V" columns						Full span					
Load case	15	16	17	22	23	24	15	16	17	22	23	24
N [kN]	-5529.9	0.24	-7340.9	-24708.8	9606.67	-12366.5	-5529.9	-6814.47	0.16	-24708.8	7680.09	-12366.48
M_1 [kNm]	-0.44	136.06	50.31	0.97	1179.32	1389.09	-0.44	-134.76	0	135.62	-1351.97	-1379.9
M_2 [kNm]	50.92	-4.23	-7857.7	-7704.71	13081.47	6808.09	50.92	12435.21	2.39	12596.23	-11627.6	-2749.6
M_3 [kNm]	-3.16	295.61	391.51	101.15	-5555.29	-5467.56	5.54	415.52	-376.68	-316.14	5413.52	5428.15
T_2 [kN]	-36.64	0.07	47.04	-158.78	440.22	394.52	36.64	43.6	0	158.75	-1618.03	-1590.35
T_3 [kN]	-0.08	0.07	0	0.23	-1327.98	-1327.96	0.03	-685.97	0	685.91	-3596.15	-3596.21
T [kN]											3943.39	
z [mm]				-3.81		-84				2.6		-78

Legend: N – Normal force, T2 - transverse force in the horizontal plane, T3 – transversal force in the vertical plane, T – Resulting transversal force above the column cross-section near in the direction of the full span, T=√(T_2^2+T_3^2), M1 - Torsion moment, M2 - vertical plane moment (around local axis 2), M3 - horizontal plane moment (around local vertical axis 3), z – vertical displacement; r1 – ring rotation

Table 3: Load cases 15, 16, 17, 22, 23, 24 – Extreme values.

Results of calculations by TOWER software are presented in Fig. 4 for load case 23 and in Figs. 5-6 for load case 24.
In Fig. 4a one can see that the higher tensile force is in the ring sections above the "V" columns. Normal force ratio in the ring is 9606.67/7677.12=1.25. Tensile force due to dead load of the dome and snow in the sections above the "V" columns

is 25% higher than the forces in the full span. Maximum value of normal force is shown in Fig. 5. In Fig. 4b one can see that the moment values in the horizontal plane in sections above "V" columns and in the full span are very similar, with a difference of only 2.6% - 5555.29/5413.52=1.026 (according to Žeželj, values were 5330 and 5360 kNm, [4]). In Fig. 4c one can see that values of maximum moments in the vertical plane in ring sections above "V" columns and the full span, are very close (12.5% difference), - 13081.47/11627.6 =1.125, although of opposite directions. In Fig. 4d one can see that the peaks above all columns are 942.47 kNm; Values immediately before these peaks are 776.98 kNm.

Results for load case 24 are shown in more detail, since they illustrate the final stage of load combinations which the structure goes through, i.e., the forces and moments for the final stage when all pre-stressing force losses Nk∞ are present, and when all cables, except the inclined ones in the support ring rib, are combined with the dead load of the dome structure, snow load and support hoop and columns.

The pre-stressing force N = -12366 kN can be read from the diagram. Due to this force, i.e., after all design force losses have occurred, for all cables except the inclined ones, as well as the dead load of the structure, the roof and snow, the resulting normal force diagram is saw-shaped, which can be clearly seen in the below Fig. 7. Maximum horizontal moment ratio above the columns and in the full span is M3=-5467.56 /5428.15 =-1.0073, the difference being only 0.73%.

Figs. 9-11 show vertical plane moments and their enlarged view in two different ways, respectively. Fig. 12 shows torsion moment diagram and its enlarged view, indicating the highest value in the full span and peaks above the "V" columns, as shown in more detail in Fig. 13. Extreme torsion moments are at approximately 1/5th of the full span, which represents a distance of around 5-5.35 m from the columns. Peaks in torsion diagrams can be seen in the sec-tions above the "V" columns.

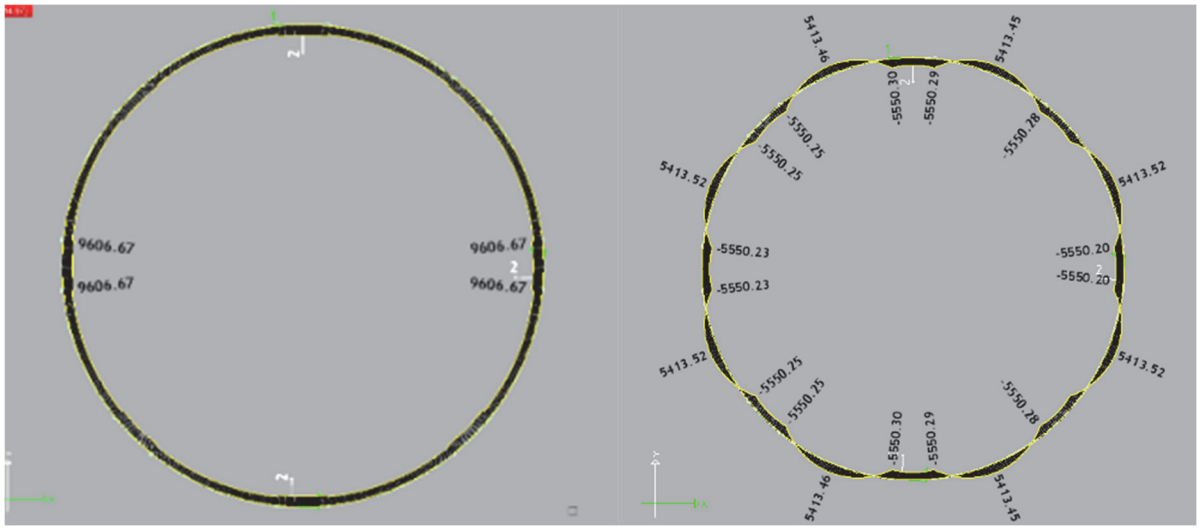

a) N=9606.67 kN; 7680.09 kN b) M3=-5555.29 kNm; 5413.52 kNm

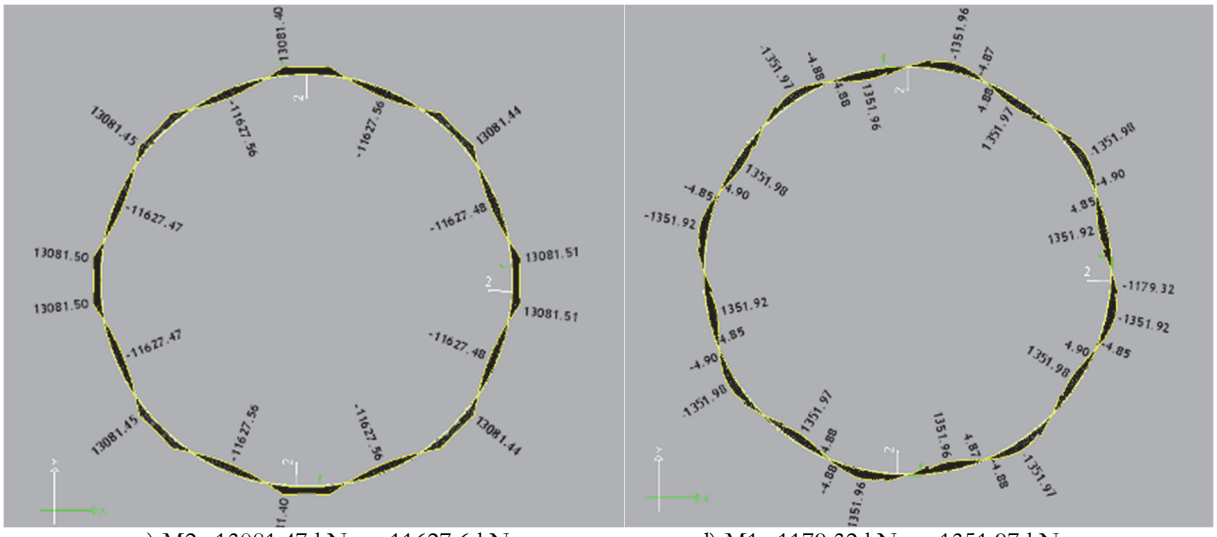

c) M2=13081.47 kNm; -11627.6 kNm d) M1=1179.32 kNm; -1351.97 kNm

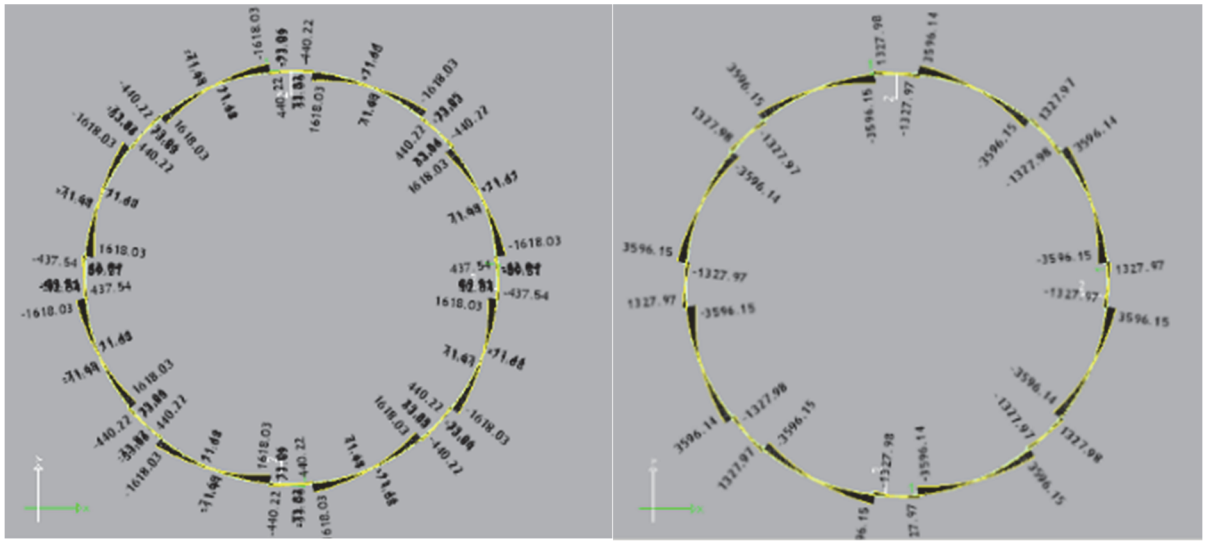

e) T2=440.22; -1618.03 kN; 0; 71.68 kN f) T3=1327.98 kN; -3596.15 kN

Figure 4: Results for load case 23.

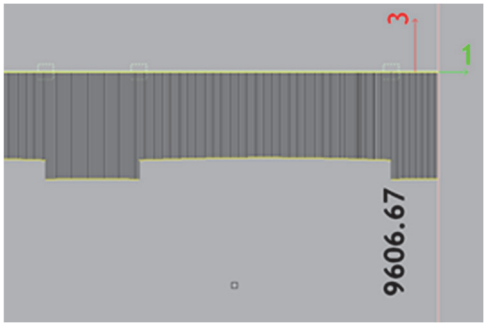

Figure 5: Maximum value of normal force –N.

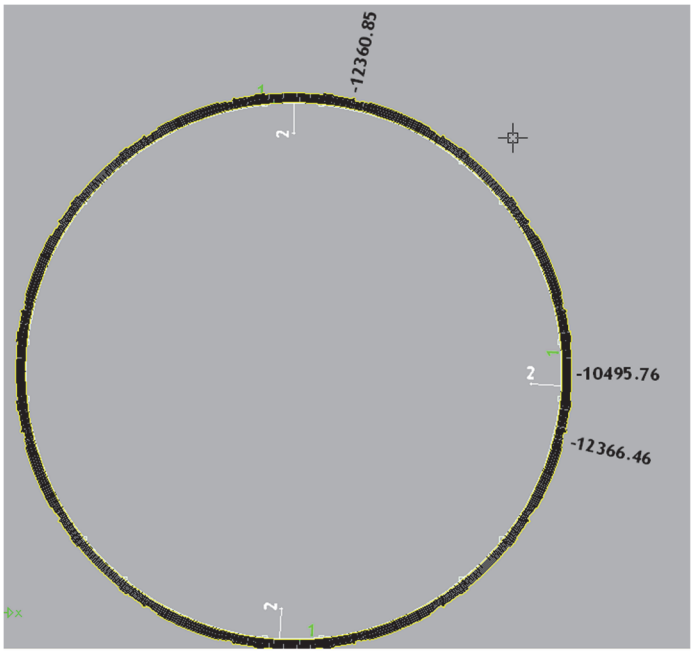

Figure 6: Normal force diagram – N.

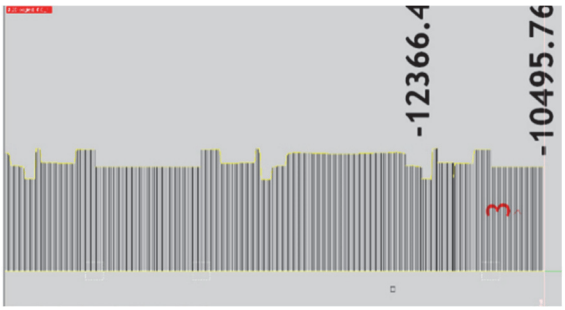

Figure 7: Enlarged portion of normal force diagram: N=-12366.46; -10496; min N=-9221.63kN.

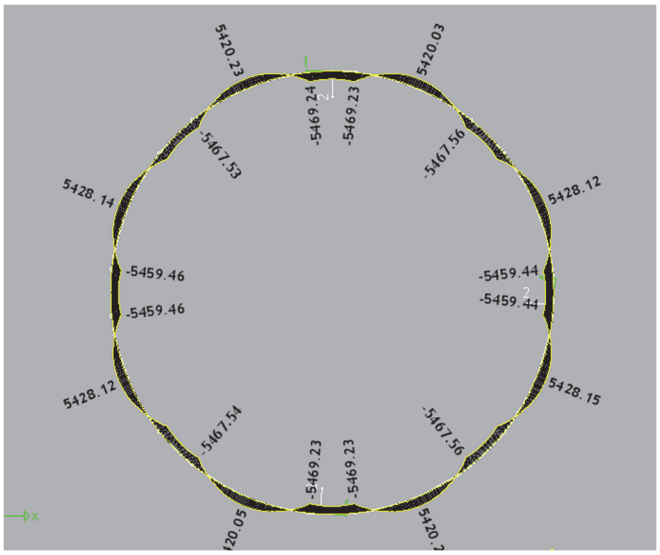

Figure 8: Horizontal plane moment diagram – M3.

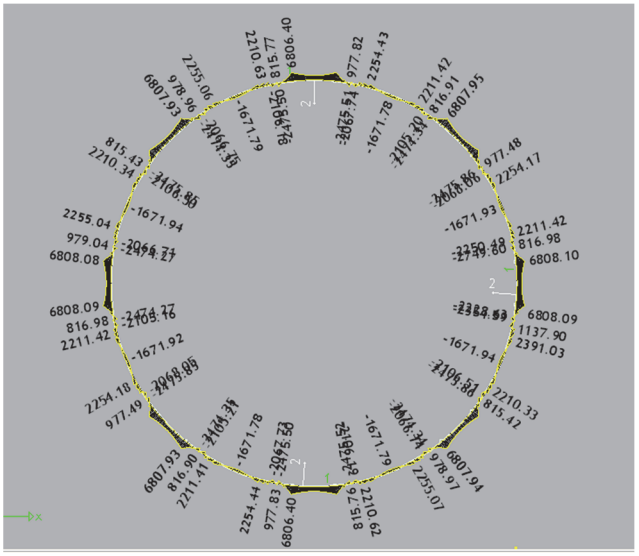

Figure 9: Vertical plane moment diagram: M2=6808.09 kNm; -283.56; 815.76; -2749.60.

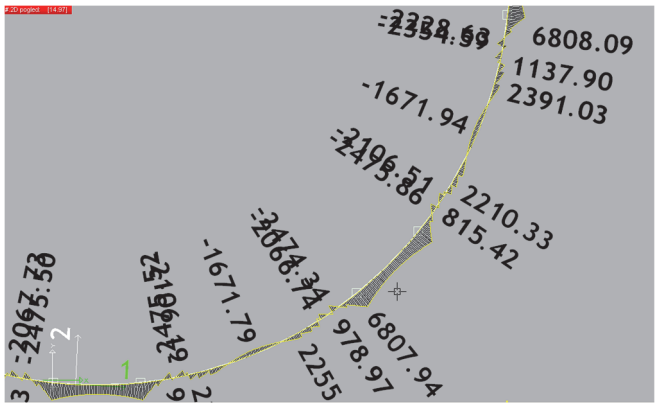

Figure 10: Enlarged portion of the vertical plane moment diagram - M2.

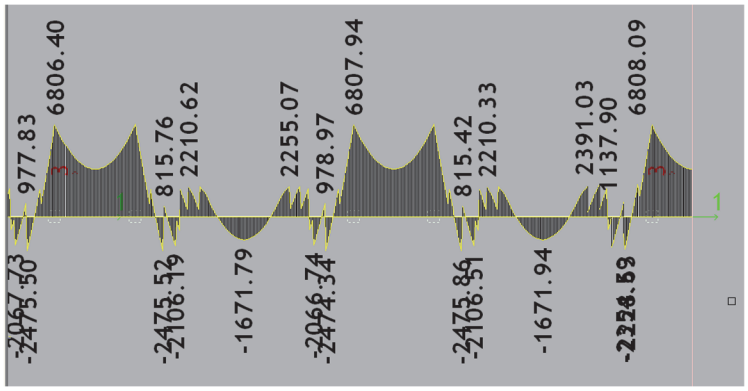

Figure 11: Enlarged portion of the vertical plane moment diagram: M2=6808.09; -2475.52; 815.42; -2106.51; 2210.33; -1671.94kN.

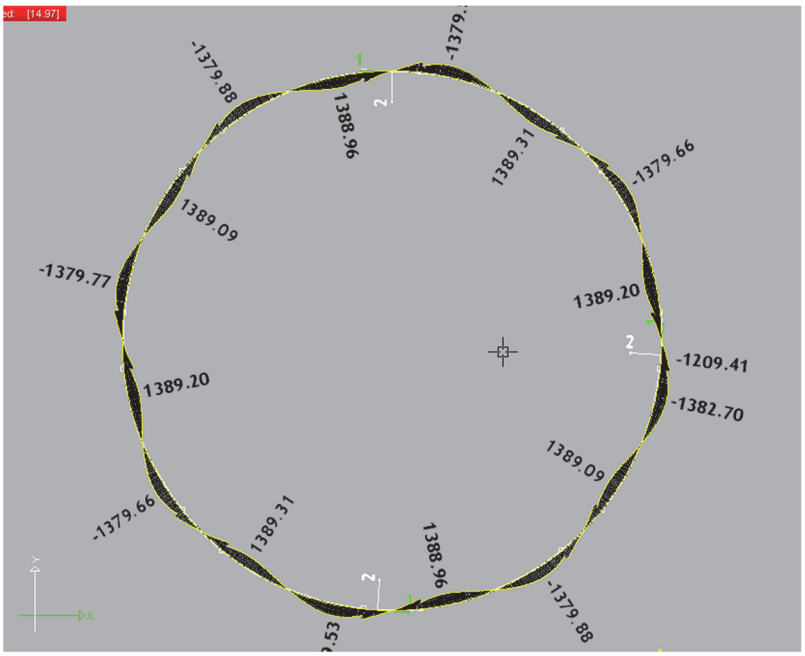

Figure 12: Torsion moment diagram M1=-1389.09 kNm; 1379,88 kNm; 1209.41 kNm.

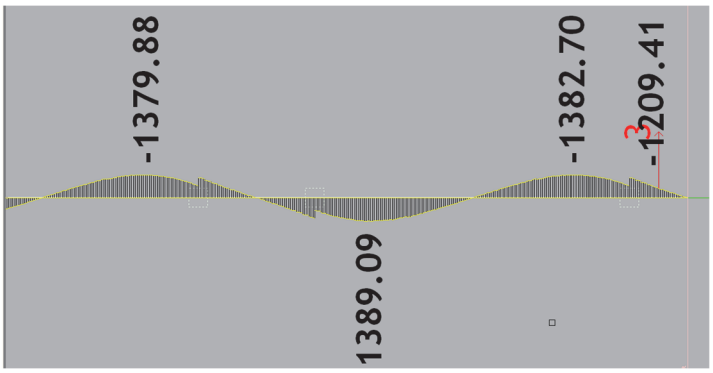

Figure 13: Enlarged portion of the torsion moment diagram - M1.

Figs. 14 and 15 show transversal force diagram in horizontal and vertical plane, respectively. Fig. 16 shows vertical displacement diagram.

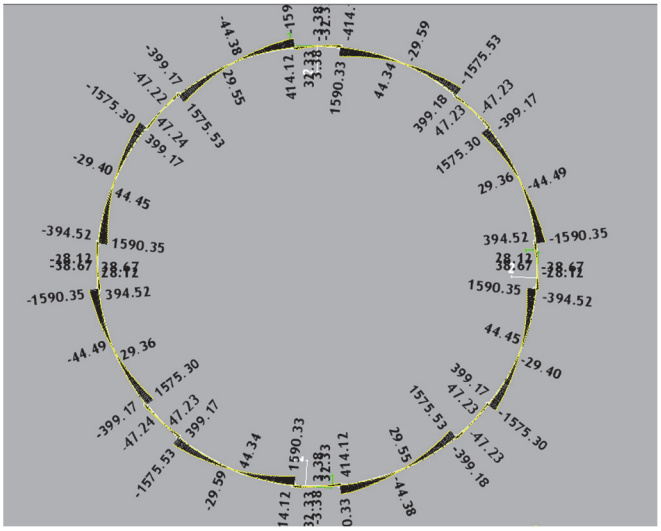

Figure 14: Transversal force diagram in the horizontal plane: T2=-394.52 kN; 1590.35 kN.

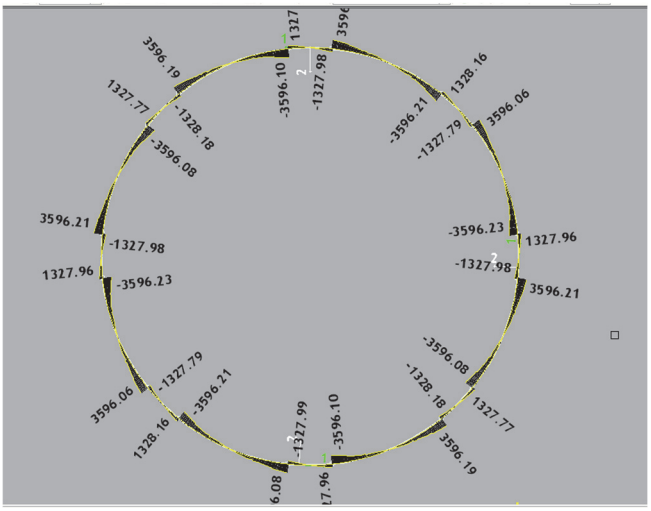

Figure 15: Transversal force diagram in the vertical plane: T3=-1327.96 kN; -3596.21 kN.

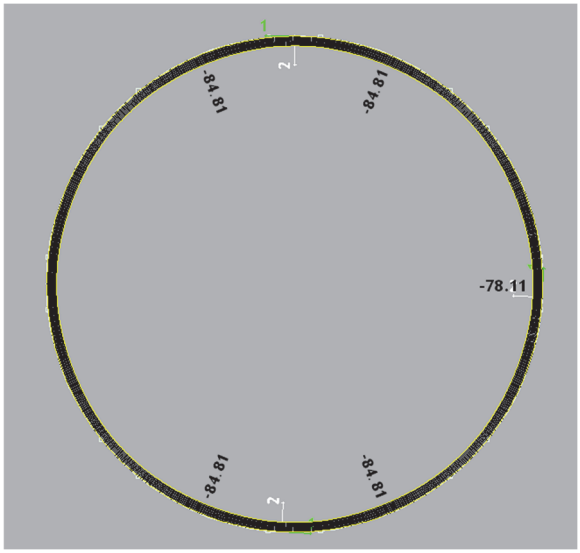

Figure 16: Vertical displacement diagram: zp=-84 mm; -78 mm.

In the load case 23 one can see that the compressive force N is larger above the "V" columns, whereas the M3 moment above all columns are close to values within the full span, but are of the opposite direction. Their values agree very well with those obtained by Žeželj, [2,5], as shown in Tab. 4. Also, values for M2 moment above "V" columns and within the span are in reasonable agreement, Tab. 4.

Area	Above the "V"columns		Full span	
	Load case 23	Žeželj results	Load case 23	Žeželj results
M_3 [kNm]	5555.29	5228.73	5413.52	5258.16
M_2 [kNm]	13081.47	10840.05	11627.6	12890.31

Table 4: Comparison between Žeželj's extreme values and load case 23 extreme bending moments.

For load case 24, compressive force N was caused by permanent pre-stressing forces, i.e., it was determined after all design force losses due to pre-stressing had occurred, for all cables except the inclined ones in the rib of the supporting hoop. In addition, compressive force N was affected by the dead weight of the structure, the roof and snow, which resulted in a saw-shaped diagram, Fig. 7. Maximum M_3 moments were also uniform, like in the previous case, Fig. 8. Contrary to that, resulting M_2 moment in the vertical plane varied considerably, from 6808 to -2750 kNm, Fig. 9. Torsion moment M_1 is also uniform in magnitude, with noticeable difference only above "V" columns, Fig. 12. Anyhow, it does change its direction (sign), Figs. 12-13. The maximum value is at 1/5th of the support hoop full span, Fig. 14.

Extended Finite Element Method simulation of crack growth in the „V" column

Following the calculations of forces, moments and support displacements, 2D extended Finite Element Method (xFEM) was used to simulate crack growth in the „V" column. For this simulation an edge crack of 2.5 mm length in one of the reinforcement bars (5 mm in diameter, made of high-strength steel) was assumed to exist. The main purpose was to determine how the column behaves with a loading defined as a 2 cm displacement of the support due to foundation sinking, corresponding to remote stress of 150 MPa. Foundation sinking was observed in one of the main ring support columns, which was then chosen for this analysis. The support column positions and locations can be seen in Fig. 17. The numerical model with the displacement corresponds to the leftmost column in the figure. The crack was located to pass first through the concrete part, and then through the steel bar. Other details of this analysis can be found in [9], whereas here focus is on von Mises stress distribution, presented in Fig. 18. Steel bar was modelled with different number of elements, from 3 to 8, to minimize the effect of mesh. One can see that the crack reached and entered the steel bar, with maximum stress values around 590 MPa at the crack tip.

Figure 17: FE Model of the support rings and "V" columns in TOWER software.

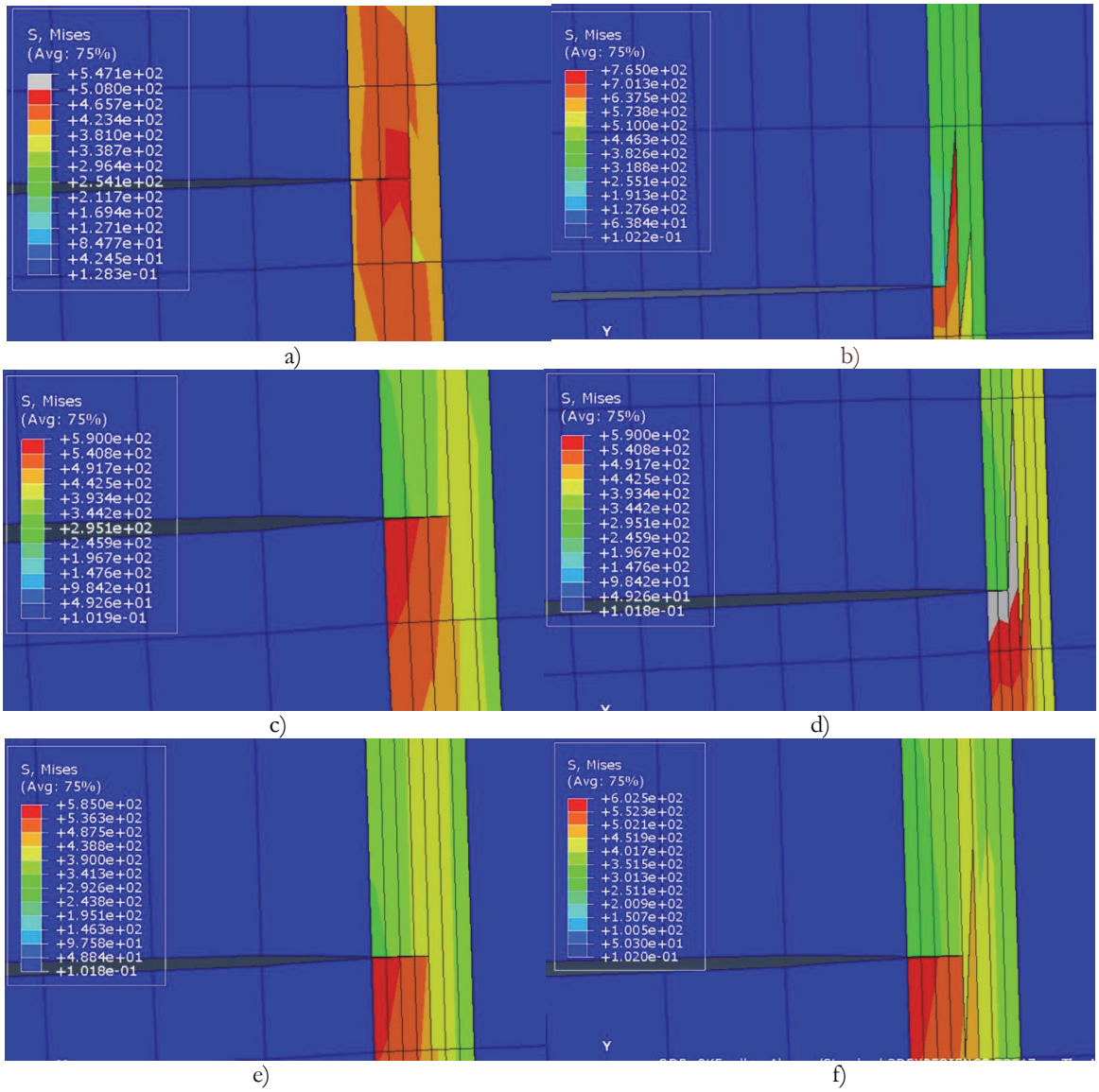

Figure 18: Results of xFEM analysis, distribution of von Mises stress, a) 3 FEs, b) 4 FEs, c) 5 FE, d) 6 FEs, e) 7 FEs, f) 8 Fes.

Discussions

As can be seen from the comparison of the results presented here for the complete Finite Element Hall 1 model, and the original ones, obtained by traditional engineering tools, [2,27,28], agreement is excellent both for the main support hoop and inclined columns. This means that the results obtained by Žeželj and his team, who did not have access to complex means of calculation, such as the FEM, are remarkable achievement.

As for the structural integrity, a simple conservative linear elastic fracture mechanics analysis can provide the minimum fracture toughness value of a bar steel to sustain an edge crack with a length up to the half bar thickness (a=2.5 mm):

$K_I=Y\sigma\sqrt{\pi a}=1139$ MPa$\sqrt{mm}$,

where K_I is the stress intensity factor, Y is the geometry factor:

$$Y(a/W)=1.12-0.26(a/W)+10.52(a/W)^2-21.66(a/W)^3+30.31(a/W)^4=2.71 \ (a/W=0.5),$$

σ=150 MPa is the remote stress, crack length a=2.5 mm. Therefore, the minimum value of a bar steel fracture toughness is 1139 MPa$\sqrt{mm}$, being 88% of the value reported in [29], K_{Ic}=41 MPa$\sqrt{m}$ =1296 MPa$\sqrt{mm}$.
More sophisticated analysis can be made by using the Failure Assessment Diagram, which takes into account not only linear elastic fracture mechanics parameters, but also a plastic collapse, quantified by the ratio σ_n/σ_c, where σn is the net stress and σ_c is the critical stress, as explained and applied in the scope of risk base assessment of structural integrity and life, [30-33].
In the scope of a conservative approach, applied here the net stress is taken as equal to the maximum value at the crack tip (590 MPa). If the critical stress is taken as the half-way between YS and TS, (1375 MPa for YS=1250 MPa and TS=1500 MPa), X coordinate is 590/1375=0.43. The Y coordinate is already defined by the ratio K_I/K_{Ic}=0.88, so the point in FAD is just below the limit curve, Fig. 19.

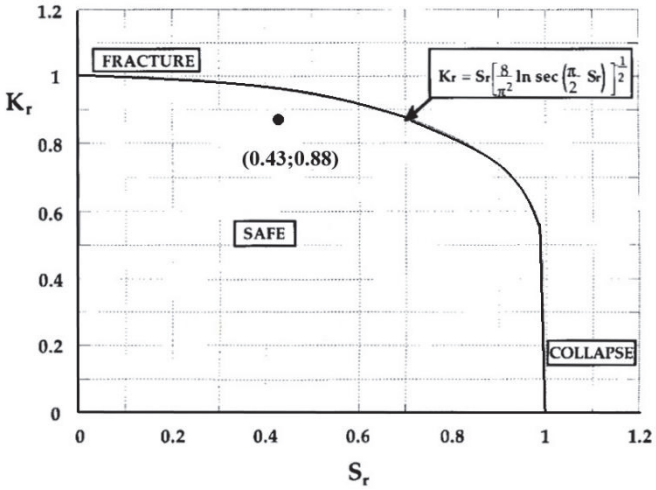

Figure 19: Failure Assessment Diagram with a point (0.43, 0.88).

As for the crack growth simulation, it can be seen that the total number of finite elements in the steel bar section provided different results in terms of crack behavior, whereas maximum stresses in the vicinity of the crack tip were similar for all cases. In the case where the crack tip was originally at the border between two elements, an unusual zig-zagging crack path was obtained; however, in the case where the crack tip was inside a finite element, the crack would propagate in a straight manner, until it reaches the next FE. Such behavior was never previously encountered by the authors, and further attention should be devoted to this unexpected effect of mesh generation on crack propagation.

Conclusions

Extensive numerical investigation shown here consisted of calculation of forces and bending moments of the Belgrade Fair Hall 1 by using TOWER software, as well as crack growth simulation by using XFEM. As for the initial position of the crack, an inclined "V" column was supposed due to the highest stresses, providing realistic results in terms of stress distribution and crack growth.
Based on the results presented in this paper, one can conclude that the approximations made in both analytical and numerical calculations had not significantly affected results. Even more importantly, one can conclude that the results obtained 60 years ago by Žeželj and his team are exceptionally accurate. Therefore, the Hall 1 remains the most prominent example of the application of concrete pre-stressing worldwide patented system IMS-Žeželj.
By using the FAD, as a simple engineering tool, structural integrity of the dome was assessed, proving that its safe operation even with a crack length reaching a half of reinforced bar thickness. This is once again, remarkable achievement for such a construction.

REFERENCES

[1] Sedmak, A., Ković, M., Kirin, S. (2022). Structural Integrity - Historical Context, Technical Gazette, 29(5), pp. 1770 – 1776, DOI: 10.17559/TV-20220321074430

[2] Zarghamee, M., Heger, F.J. (1983). Buckling of Thin Concrete Domes, ACI Journal Proceedings., 80(6), pp. 487-500 DOI:10.14359/10870

[3] Ashar, H., Naus, D.J. (1983) Overview of the use of prestressed concrete in U.S. nuclear power plants, Nuclear Engineering and Design. 75(3), pp. 425-437

[4] Petrović, G., Aranđelović, B., Flajs, Ž., Ivanković, B., (2023). Contemporary role of the ims institute in construction, reconstruction, rehabilitation and maintenance of civil structures and buildings, Structural Integrity and Life, 23, Special Issue, pp. 69-71

[5] Moncarz, P.D., Griffith, M., Noakowski, P. (2007). Collapse of a Reinforced Concrete Dome in a Wastewater Treatment Plant Digester Tank, Journal of Performance of Constructed Facilities, 21(1). DOI: 10.1061/(ASCE)0887-3828(2007)21:1(4)

[6] Jelić, M., Sedmak, A. (2020). The largest pre-stressed concrete Dome in the world – the case study of "Hall 1 of the Belgrade Fair", Procedia Structural Integrity, 28, pp. 1833-1838. DOI:1016/j.prostr.2020.11.006

[7] Žeželj, B. A. (1960). Large Dome at Belgrade, Concrete and Constructional Engineering. 7, pp. 263–270.

[8] Jevtić, D. (1957). Pre-stressed concrete, Belgrade, Gradjevinska knjiga.

[9] Jelić, M., Sedmak, A., Sedmak, S. Folić, B., Folić, R. (2021). Numerical simulation of "Hall 1 of the Belgrade Fair", Engineering Failure Analysis, 127, 105570, DOI: 10.1016/j.engfailanal.2021.105570.

[10] Pavišić, M. (2021). Concrete deterioration, consequences, integrity and bearing capacity assessment of in-service concrete bridges, Structural integrity and life, 21(2), pp. 131–133.

[11] Milovanović, A., Martić, I., Trumbulović, Lj., Diković, Lj., Drndarević, B. (2021). Finite element analysis of spherical storage tank stress state, Structural Integrity and Life, 21(3), pp. 273-278.

[12] Milovanović, A., Mijatović, T., Diković, Lj., Trumbulović, Lj., Drndarević, B. (2021). Structural integrity analysis of a cracked pressure vessel, Structural Integrity and Life, 21(3), pp. 285-289.

[13] Zaidi, R., Sedmak, A., Kirin, S., Grbovi ć, A., Li, W., Lazić Vulićević, Lj., Šarkočević, Z. (2020). Risk assessment of oil drilling rig welded pipe based on structural integrity and life estimation, Engineering Failure Analysis, 112, 104508, DOI: 10.1016/j.engfailanal.2020.104508

[14] Aranđelović, M., Sedmak, S., Jovičić, R., Perković, S., Burzić, Z., Đorđević, B., Radaković, Z. (2021). Numerical simulation of welded joint with multiple various defects, Structural Integrity and Life, 21(1), pp. 103-107

[15] Aranđelović, M. Sedmak, S., Jovičić, R., Perković, S., Burzić, Z., Radu, D., Radaković, Z. (2021) Numerical and experimental investigations of fracture behaviour of welded joints with multiple defects, Materials, 14(171), 4832, DOI: 10.3390/ma14174832.

[16] Banks-Sills, L., Sedmak, A. (2020). Linear elastic and elasto-plastic aspects of interface fracture mechanics, Structural Integrity and Life, 20(3), pp. 203-210.

[17] Mijatović, T., Milovanović, A., Sedmak, A., Milović, Lj., Čolić, K. (2019). Integrity Assessment of Reverse Engineered Ti-6Al-4V ELI Total Hip Replacement Implant, Structural Integrity and Life, 19(3), pp. 237-242.

[18] Radu, D., Sedmak, A., Sedmak, S., Dunjić, M. (2018) Stress analysis of steel structure comprising cylindrical shell with billboard tower, Tehnicki Vjesnik, 25(2), pp. 429-436, DOI: 10.17559/TV-20160819201538.

[19] Đurđević, Đ., Sedmak, S., Đurđević, A., Anđelić, N., Maneski, T. (2021). Development and calculation of supporting structure for mining power equipment, Structural Integrity and Life, 21(2), pp. 173-177.

[20] Lagerblad, U., Wentzel, H., Kulachenko, A. (2021). A methodology for strain-based fatigue damage prediction by combining finite element modelling with vibration measurements, Engineering Failure Analysis, 121, 105130, DOI: 10.1016/j.engfailanal.2020.105130.

[21] Hanganu, A.D., Oñate, E., Barbat, A.H. (2002). A finite element methodology for local/global damage evaluation in civil engineering structures, Computers & Structures, 80(20-21), pp. 1667-1687.

[22] Milovanović, N., Sedmak, A., Arsić, M., Sedmak, A., Božić, Ž. (2020). Structural integrity and life assessment of rotating equipment, Engineering Failure Analysis, 113, 104561, DOI: 10.1016/j.engfailanal.2020.104561.

[23] Solob, A., Grbović, A., Božić, Ž., Sedmak, S. (2020). XFEM based analysis of fatigue crack growth in damaged wing-fuselage attachment lug, Engineering Failure Analysis, Vol. 112, 104516, DOI: 10.1016/j.engfailanal.2020.104516.

[24] Kraedegh, A., Li, W., Sedmak, A., Grbović, A., Trišović, N., Mitrović, R., Kirin, S. (2017). Simulation of Fatigue Crack Growth in A2024-T351 T Welded Joint, Structural Integrity and Life, 17(1), pp. 3-6.

[25] Kraedegh, A., Li, W., Sedmak, A., Grbović, A., Trišović, N., Mitrović, R., Kirin, S. (2017). Simulation of Fatigue Crack Growth in A2024-T351 T Welded Joint, Structural Integrity and Life, 17(1), pp. 7-10.
[26] Jovičić, G., Živković, M., Jovicic N., Milovanović D., Sedmak A. (2010). Improvement of algorithm for numerical crack modelling, Archives of Civil and Mechanical Engineering, 10 (3), pp. 19–35, DOI: 10.1016/s1644-9665(12)60134-4.
[27] Jelić, M. (2017). Common characteristics of main contributions of Roger Boscovich, Milutin Milanković and Branko Žeželj to the development of civil engineering, Structural Integrity and Life, 17(2), pp. 157─169.
[28] Jelić, M. (2017). Continuity in spreading of Serbian civil construction technology for the period from 1957 till today: Patents with domestic and worldwide application, Proceedings Technology, Culture and development 24, Akademska misao, Belgrade, pp. 7─31.
[29] Elices, M., Perez-Guerrero, M., Iordachescu, M., Valiente, A. (2017). Fracture toughness of high-strength steel bars, Engineering Fracture Mechanics 170, pp.119–129, DOI: 10.1016/j.engfracmech.2016.12.001.
[30] Zaidi, R., Sedmak, A., Kirin, S., Grbovic, A., Li, W., Lazic Vulicevic, Lj., Sarkocevic, Z. (2020). Risk assessment of oil drilling rig welded pipe based on structural integrity and life estimation, Engineering Failure Analysis 112, 10450, DOI: 10.1016/j.engfailanal.2020.104508.
[31] Golubović, T., Sedmak, A., Spasojević Brkić, V., Kirin, S., Rakonjac, I. (2018). Novel risk based assessment of pressure vessels integrity, Technical Gazette, 25(3), pp. 803 – 807, DOI: 10.17559/TV-20170829144636.
[32] Milovanović N., Sedmak A., Arsic M., Sedmak S.A., Božić Z. (2020). Structural integrity and life assessment of rotating equipment, Engineering Failure Analysis, 113, 104561, DOI: 10.1016/j.engfailanal.2020.104561.
[33] Radu, D., Sedmak, A., Sedmak, S., Li, Wei. (2020). Engineering critical assessment of steel shell structure elements welded joints under high cycle fatigue, Engineering Failure Analysis, 114, 104578, DOI: 10.1016/j.engfailanal.2020.104578.